# Fluidic mechanism for dual-axis gyroscope

Van Thanh Dau[1†*], Thien Xuan Dinh[2†], Canh Dung Tran[3,4†], Phong Nhu Bui[5], Du Dinh Vien[5] and Hoa Thanh Phan[6*]

[1] Research Group (Environmental Health), Sumitomo Chemical. Ltd, Hyogo 665-8555, Japan
[2] Graduate School of Science and Engineering, Ritsumeikan University, Shiga 525-8577, Japan
[3] School of Mechanical and Electrical Engineering, University of Southern Queensland, Australia
[4] Department of Mechanical Engineering, National University of Singapore, Singapore
[5] Faculty of Electronic Engineering, Hanoi University of Industry, Hanoi, Vietnam
[6] HaUI Institute of Technology, Hanoi University of Industry, Hanoi, Vietnam
[†] *Co-first authors (equal contribution)*
[*] *Corresponding authors:* dauv@sc.sumitomo.co.jp and phanthanhhoa@haui.edu.vn

**Abstract**

In this paper, we report a further study of flow-network generating four jet flows which circulate in a sealed device to experimentally investigate the feasibility and efficiency of a dual-axis gyroscope. The experiment is carried out successfully and the experimental results reasonably agreed with those obtained by numerical analysis using OpenFOAM. The flow rectifying coefficient is determined using the mathematical lump model for a vibrating system, which takes into account of the device geometry and resonant frequency. Experimental and numerical results demonstrate that the coefficient of the new system developed in this study is significantly higher than those of conventional designs. The hotwire-integrated device which can function as a dual-axis gyroscope is tested using a turntable with speeds up to 1900 rpm. The scale factor and cross-sensitivity of the system are 0.26 μVs/° and 1.2 %, respectively. The cross-sensitivity and the effects of linear acceleration, actuating voltage on the diaphragm, heating power and position of hotwires are also investigated.

Keywords: fluidic gyroscope, lump model, jet flow circulation, resonant frequency, hotwire, 3D transient simulation

NOMENCLATURE

| | | | |
|---|---|---|---|
| $\vec{u}$ | Velocity vector of fluid | $\omega$ | Angular velocity |
| $p$ | Pressure | q | Uniform distributed force |
| $\rho$ | Density | K | Equivalent spring stiffness |
| $\vartheta$ | Kinematic viscosity | M | Equivalent mass |
| $z(r, t)$ | Diaphragm deformation | Q | Flow rate |
| $\nu$ | Poisson's ratio | $\Gamma_D$ | Kinetic energy of diaphragm |
| $Z(t)$ | Central deflection of diaphragm | $\Gamma_F$ | Kinetic energy of fluid |
| $\varphi(r)$ | Shape of deformation | $P$ | Pressure force |
| $f$ | Frequency of applied force | $U_c(x)$ | Velocity at center of nozzle |
| $\delta$ | Amplitude of central deflection of diaphragm | $a$ | Radius of diaphragm |
| $E$ | Young's modulus | $Q_P$ | Time average deformation |
| h | Thickness of diaphragm | $\alpha$ | Temperature coefficient of resistance |
| $\eta$ | Rectification coefficient | $r_t$ | Radius of turntable |

## 1. INTRODUCTION

Flow in a closed system possesses several advantages, for example minimizing the number of analyzed samples [1], [2], improving the mixing [3]–[5] and the cooling [6]–[8], and a partial or complete freedom from the contamination by environmental variations [9], [10]. With the introduction of circulatory flow, the integration and miniaturization of measuring systems significantly enhance the capability and impact of microfluidic systems [11]–[15]. A majority of applications of circulatory flow in a confined space are in the inertial sensing and particular angular rate sensing where the advantage of a self-contained valveless micropump reduces the risk of damage to mechanical counterparts [16]–[19]. For such applications, many different approaches were developed to generate a jet flow. Among them, several typical techniques can be cited as follows. A lead zircona-titanate (PZT) diaphragm is used to create a continuous direct flow which is then rectified into suitable chambers [20]–[22]. Alternatively, a jet flow can be released using an electro-conjugate fluid, where it is activated by electrohydrodynamics in a high electric field between two electrodes submerged in a liquid [23]–[25]. Another method, arguably the most common actuating source in fluidic inertial sensors, is based on the natural convection from a locally heated region where a jet flow moves along the direction of mass diffusion [26]–[31]. In addition, the thermal expansion, which is marginally dissimilar from the natural convection method, is also applied to generate the kinetics of fluid flows. For this approach, propelled by the gas expansion from a source heated with a high rate, the thermal expansion is not dependent on the gravity until the air movement transfers from an expansion state

to a diffusion one [32]–[35]. Finally, the vortex flow based inertial sensor using two external pumps as a flow source was reported recently [36], [37].

Although the natural convection based fluidic gyroscope possesses application potential, it is not stable while working with a linear acceleration. However, this drawback can be overcame using the convection force based fluidic gyroscope with a jet flow. Indeed, the effect of gravity on the free floated jet flow is neglected in a media. Using this approach, we recently developed the single- and dual-axis fluidic gyroscopes using the conventional production methods [38]–[41] in which the dual axis one includes an aluminum cylinder assembled by dozen of conventional mechanical parts, a pump and a hotwire sensing [40]. For the gyroscope using this principle, the effect of gravity on the free floated jet flow is neglected. Furthermore, this gyroscope can sense up to an angular rate of 3000 °/s with a cross-sensitivity of 0.25 % between two axes.

Experimental results shown that although the principle of the fluidic gyroscope and its configuration are relatively simple, there are certain limits in the fundamental design due to the cumbersome and high cost of the device. Several alternative techniques such as using planar overlapping layers are applied to simplify the fabrication process, but difficulties in the theoretical design are still existent [42], [43]. Thus, several ideas, such as the introduction of PZT pumping using microfabrication process to the fluidic gyroscope, were recently published. However, so far those works are lack of either the necessary experimental investigation [44] or the pumping integration [45].

In this work, a modified convection force based fluidic gyroscope with a jet flow is developed based on the structure of '*a flow network*'. In this new system, the velocity of flow is determined using two hotwires installed in each sensing chamber. The present device, whose feasibility and efficiency are experimentally investigated, is simple in manufacturing and easy in operating. In order to evaluate the device efficiency, a model is proposed to characterize the rectifying ratio of the jet flow circulator valveless pumping system, followed by theoretical and experimental studies of a piezo-electrically actuated microfluidic device. The inertial sensing ability of the system is also investigated using a turntable, and the effect of several governing parameters was also assessed.

## 2. DEVICE DESCRIPTION AND FLOW SIMULATION

### 2.1 MECHANISM OF DEVICE

The principle of a flow chip was reported elsewhere [43], [46] and is summarized here as follows. A disk pump chamber with a diameter of 18 mm and a depth of 0.3 mm, activated by a PZT diaphragm is located at the top center. Beneath the pump chamber, a symmetric flow network about the vertical axis is installed, which consists of four driving channels and four associated sensing chambers. Each driving channel and its sensing chamber are connected to each other by a channel at the outermost point of the chip and then linked to the pump chamber at another end. The junction of driving channel, sensing chamber, and pump chamber forms a rectifying nozzle as illustrated in Figs. 1 and 2.

For a working cycle, when the diaphragm shifts down, air from the pump chamber is compressed through a rectifying nozzle to flow into a driving channel to accumulate a momentum, and then propagates to the outer end of the sensing chamber. When the diaphragm shifts up, owing to the specific nozzle geometry and accumulated momentum in the driving channel, air flow moves from the inner ends of the sensing chamber toward the rectifying nozzle and accumulates more momentum in the driving channel. Such asymmetric flow is continuously rectified into a circulating flow inside the system, as described in Fig. 2. After each cycle of the propagation, the flow velocity further increases until reaching a stable state.

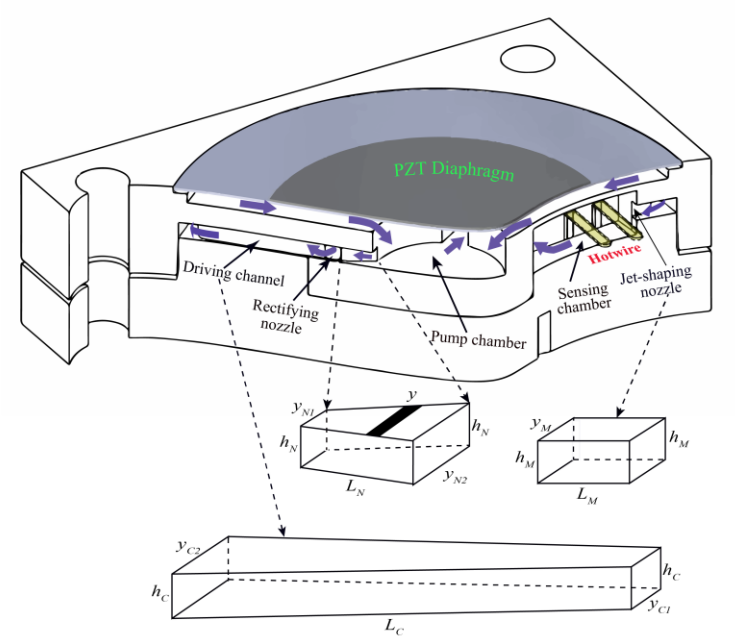


Figure 1. Mechanism of system illustrated by device overview and cut-views: arrows indicate flow direction starting from pump chamber, leading through rectifying nozzle, driving channel, jet-shaping nozzle, and sensing chamber, and then returning to rectifying nozzle for the subsequent circulation. The insets illustrate shapes of rectifying nozzle, driving channel, and jet shaping nozzle.

At the junction of the nozzle, the cross-section of the two opposite inlets is designed larger than one of the outlets, which yields a lower fluidic resistance at the inlets than one at the outlets. Driving channels are centrifugally diverged in the fan-shaped channels with an open angle of 6° and depth of 0.5 mm. Meanwhile working chambers are centripetally converged with an angle of 12° and depth of 1.5 mm where the flow assumes the shape of a jet through a jet-forming nozzle in accordance with the geometry of the chamber. The sensing element includes two tungsten hotwires which are vertically centered and crossed over each sensing chamber (Fig. 1).

## 2.2 Numerical simulation of flow

Since the flow is self-generated in a closed network, it is a compressible flow and governed by the system of conservation equations as follows.

$$\frac{\partial \rho}{\partial t} + \nabla \cdot \rho\vec{u} = 0 \tag{1}$$

$$\frac{\partial \rho\vec{u}}{\partial t} + (\vec{u} \cdot \nabla)\rho\vec{u} = -\nabla p + \nabla \cdot (\mu\nabla\vec{u}) - 2\rho\vec{\omega} \times \vec{u} \tag{2}$$

$$\frac{\partial \rho c_p T}{\partial t} + (\vec{u} \cdot \nabla)\rho c_p T = \nabla \cdot (\lambda\nabla T) \tag{3}$$

where $\vec{u}$, $p$, and $T$ are the velocity, pressure, and temperature of the flow, respectively. The second term at the RHS of Eq. (2) $2\rho\vec{\omega} \times \vec{u}$ represents the Coriolis's apparent acceleration of a rotating frame with the angular velocity $\vec{\omega}$, $\mu = 1.789 \times 10^{-5}$ Pas , $\rho = 1.2041$ kgm$^{-3}$ , $\lambda = 24.2 \times 10^{-3}$ Wm$^{-1}$K$^{-1}$, and $c_p = 1006.43$ Jkg$^{-1}$K$^{-1}$ are the specified dynamic viscosity, density, thermal conductivity, and specific heat of the air, respectively.

The pressure ($p$) and density ($\rho$) satisfy the state equation $p = \rho R_u T/M_w$ where $R_u = 8.314$ Jmol$^{-1}$K$^{-1}$ and $M_w = 28.96$ gmol$^{-1}$ are the universal gas constant and the molecular weight, respectively.

The boundary condition imposed on the diaphragm is derived from its vibrating rate $v(\vec{r}, t)$ and the shape function $\varphi(r)$ as follows.

$$v(\vec{r}, t) = 2\pi f Z \cos(2\pi f t)\, \varphi(\vec{r}), \tag{4}$$

$$\varphi(r) = (1 - (r/a)^2)^2, \tag{5}$$

where $a$ = 10 mm is the diaphragm radius. The PZT diaphragm whose boundary conditions are described in Eq. (4) is considered as the inlet surface.

For the simulation, the problem governed by Eqs (1)-(3) and boundary conditions with Eqs. (4)-(5) is solved numerically using our program code developed in OpenFOAM environment. In this program, the semi-implicit method is to discretize Eqs. (1)-(3) for the couple of pressure–velocity using pressure linked equations (SIMPLE).

In order to ensure the simulation stability, the discretization equations are advanced with time using the first-order Euler time stepping method. Meanwhile, for the spatial discretization, the second-order upwind scheme is used to accurately capture the flow field at each time step. The general version of the algebraic multigrid method, which is a fast and stable scheme for elliptic equations, is applied to determine the pressure field of the flow.

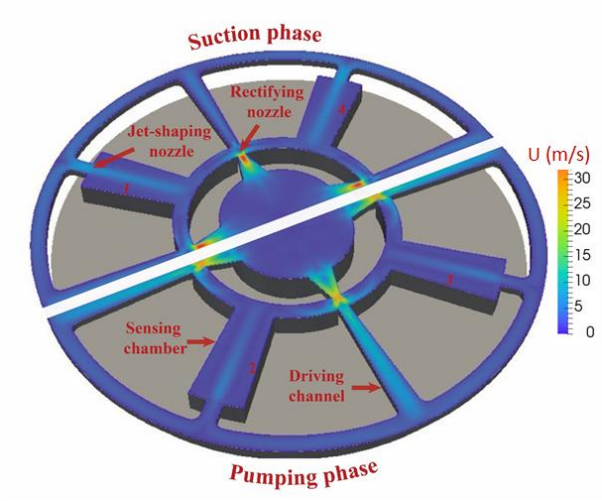


Figure 2. Simulation of flow generated inside device in two phases: (i) Pumping phase (Top half): compressed air flows from pump chamber to driving channel through rectifying nozzle and gains momentum at the outer end of the sensing chamber; (ii) Suction phase (Bottom half): circulating air flow sucked from the inner ends of the sensing chamber is accumulated into the flow in driving channel to accelerate the flow. The momentum of flow increases over a cycle.

Numerical results of flows in the pumping phase and suction phase illustrated in Fig. 2 are used as the pumping principle as described in section 2.1. Several simulated results of flow in sensing chamber will be presented in section 4 together with experimental results.

### 2.3 Estimation of the pump's rectified performance using the lump model

Although a nozzle of the circulatory flow was designed, its rectifying coefficient has not been sufficiently considered in our last publications. In this work, the rectifying ratio of the nozzle developed in our present device is studied based on the dynamic characteristics of the flow. As the jet flow is generated by the vibration of a PZT diaphragm, the resonant frequency response is a critical parameter. The diaphragm's vibration pushes and pulls the air through the nozzle to generate flow. In other words, the kinetics of the device apparently depends on the vibration of the diaphragm, which generates the flow inertia in the system.

As illustrated in Fig. 2, the effect of air inertia on the device's kinetics strongly depends on the rectifying nozzle, driving channel, and jet shaping nozzle. So, with a nozzle of reasonable rectifying coefficient, a large volume of air is rectified when flowing through the nozzle and the driving channel, and the air flow subsequently reaches the main chamber. Hence, the device receives high air inertia while the resonant frequency of the system is low. In contrast, if less air flows through the nozzle then air inertia in the driving channel and sensing chamber decreases, and the resonant frequency is high. Therefore, the ratio of the air flow rate through the driving channel to the volume variation of air generated in a cycle of the diaphragm's vibration, called as the rectification efficiency, is used to determinate the resonant frequency of the system.

Consider the device as a vibration system, the resonant frequency $f_o$ is expressed by

$$f_o = \frac{1}{2\pi}\sqrt{\frac{K}{M}}, \tag{6}$$

where $M$ and $K$ are the equivalent mass and stiffness of the system, respectively. The rectifying coefficient is then calculated based on the approximation of $K$ and $M$ as follows.

In a cycle of vibration, the volume variation of air caused by the diaphragm ($dV = Z\int_0^a \phi(r)2\pi r dr$, order of $1 \times 10^{-3}$ cm$^3$) is marginal in comparison with the total volume $V$ ($V$ = 1.3 cm$^3$) of the device. Therefore, the air compressibility is negligible. Thus, the stiffness K can be modeled as the ratio of the generating force $F$ by PZT diaphragm to its center displacement $Z$ ($K = F / Z$). The displacement and force at the center of a circular diaphragm under uniformly distributed load $q$ is determined by Eqs. (7) and (8), respectively [47], [48]:

$$Z = 3qa^4(1-\nu^2)/(16Eh^3), \tag{7}$$

$$F = q\pi a^2, \tag{8}$$

where *E*, ν, *a*, *h* are defined in the nomenclature above. The equivalent spring stiffness *K* is then estimated by

$$K = \frac{F}{Z} = \frac{16}{3}\frac{Eh^3}{\pi a^2(1-\nu^2)} \quad (9)$$

Table 1: Diaphragm and fluid network parameters

| Component | Symbol | Value | Component | Symbol | Value |
|---|---|---|---|---|---|
| Diaphragm | h (mm) | 0.2 | Driving channel | $y_{C1}$ (mm) | 0.32 |
| | A (mm) | 10 | | $y_{C2}$ (mm) | 0.8 |
| | *E* (GPa) | 100 | | $L_C$ (mm) | 4.0 |
| | ν | 0.33 | | $h_C$ (mm) | 0.5 |
| | $\rho_D$ (kg/m$^3$) | 8960 | Nozzle | $y_{N1}$ (mm) | 0.3 |
| Main nozzle | $y_M$ (mm) | 0.5 | | $y_{N2}$ (mm) | 0.8 |
| | $L_M$ (mm) | 0.7 | | $L_N$ (mm) | 1.0 |
| | $h_M$ (mm) | 0.5 | | $h_N$ (mm) | 0.5 |

With the parameters of the diaphragm given in Table 1, the equivalent spring stiffness *K* calculated by Eqs. (7)-(9) is 157.27 × 10$^3$ N/m. Meanwhile, the equivalent mass (*M*) of the system can be approximated based on the total kinetic energy ($\Gamma_{PZT}$) of the diaphragm and air flow in the device. With a given velocity of the diaphragm center ($\dot{Z} = 2\pi f Z\cos(2\pi f t)$), density of diaphragm $\rho_D$, and radius $r$ of a position on the diaphragm, the kinetic energy of the diaphragm is determined by integrating Eq. (4) as follows.

$$\Gamma_{PZT} = \frac{1}{2}\int_0^a \dot{Z}^2\,\rho_D\,\varphi^2(r)2\pi r dr \quad (10)$$

Using $\varphi(r)$ given in Eq. (5), few straightforward calculations yield $\Gamma_{PZT} = \frac{1}{2}\rho_D\pi a^2\,h/5\,\dot{Z}^2$. From the definition of kinetic energy, the equivalent mass of the diaphragm is expressed by

$$M_{PZT} = \frac{1}{5}\rho_D\pi a^2 h \quad (11)$$

Substituting the parameters listed in Table 1 into Eq. (11) yields $M_{PZT}$ = 1.016 × 10$^{-4}$ kg.

Similarly, the kinetic energy of the air flow $\Gamma_{Air}$ in the device is expressed as follows.

$$\Gamma_{Air} = 1/2\int_V u^2\,\rho_a dV, \quad (12)$$

where $\rho_a$ is the density of air flow, *V* the volume of the device, and *u* the velocity of air flow.

As presented above, a high proportion of the kinetic energy comprises the kinetic energies of flow in the rectifying nozzle ($\Gamma_{rN}$), driving channel ($\Gamma_C$), and jet forming nozzles ($\Gamma_{jN}$). The velocities of air flow in those components are substantially higher than those in the other components of system.

Let $Q_{rN}$ be the flow rate of air through a nozzle and $u = Q_{rN}/(yh_N)$ the velocity at a distance *x* from the nozzle as described in Fig. 1, the kinetic energy of air flow in the nozzle is expressed as follows.

$$\Gamma_{rN} = \frac{1}{2}\int_0^{L_N}\rho_a\frac{Q_{rN}^2}{yh_N}dx = \frac{1}{2}\rho_a\frac{Q_{rN}^2}{h_N}\int_0^{L_N}\frac{dx}{y} \quad (13)$$

As there are four nozzles, the flow rate of air through each nozzle $Q_{rN}$ is determined by

$$Q_{rN} = \frac{1}{4}Q = \frac{1}{4}\dot{Z}\int_0^a \phi(r)2\pi r dr \quad (14)$$

With $\int_0^{L_N} dx/y = \frac{L_N}{y_{N2}-y_{N1}} ln\frac{y_{N2}}{y_{N1}}$ and $K_v = \int_0^a \phi(r)2\pi r dr = \frac{1}{3}\pi a^2$, the equivalent mass of air flow through each nozzle is expressed as

$$M_{rN} = \frac{1}{16}\rho_a\frac{K_v^2}{h_N}\frac{L_N}{(y_{N2}-y_{N1})}ln\left(\frac{y_{N2}}{y_{N1}}\right) \quad (15)$$

Here, the rectifying coefficient $\eta$ at the nozzle is defined as the ratio of flow rate of air through the nozzle ($Q_{rN}$) to the flow rate through the driving channel ($Q_c$). The equivalent mass of air flowing through the driven channel is similarly determined as follows.

$$M_C = \frac{1}{16}\rho_a \frac{\eta^2 K_v^2}{h_C} \frac{L_C}{(y_{C2}-y_{C1})} ln\left(\frac{y_{C2}}{y_{C1}}\right) \quad (16)$$

The last component contributing into the equivalent mass is the air flow through the jet shaping nozzle. Since it flows through the driving channel $Q_C$ whose jet nozzle has a uniform cross section, the kinetic energy is computed by $E_M = 0.5\rho_G Q_C^2 \frac{L_M}{h_M y_M}$. Therefore, the equivalent mass contributed by the air flow through the jet shaping nozzle is given by

$$M_{jN} = \frac{1}{16}\rho_a \frac{\eta^2 K_v^2}{h_M} \frac{L_M}{y_M} \quad (17)$$

From Eqs. (11) and (15)–(17), the total equivalent mass of the device including the masses of the diaphragm, air flows through the four nozzles, driving channels, and jet nozzles is determined by

$$M = \frac{1}{5}\rho_D \pi a^2 + \frac{1}{4}\rho_a \left[\frac{K_v^2}{h_N \alpha_N} ln\left(\frac{y_{N2}}{y_{N1}}\right) + \frac{\eta^2 K_v^2}{h_C \alpha_C} ln\left(\frac{y_{C2}}{y_{C1}}\right) + \frac{\eta^2 K_v^2}{h_M y_M}\right] \quad (18)$$

The use of Eq. (9) for the equivalent spring stiffness *K* and Eq. (18) yields the relationship between the resonant frequency of the system and the rectifying efficiency of the nozzle. Hence, the pumping effect of this closed system is expressed as follows.

$$\mathrm{A} + \mathrm{B}\eta^2 = \mathrm{C}/f^2 , \quad (19)$$

with $\mathrm{A} = \frac{\rho_D \pi a^2}{5} + \frac{\rho_a K_v^2}{4 h_N \alpha_N} ln\left(\frac{y_{N2}}{y_{N1}}\right)$; $\mathrm{B} = \frac{K_v^2 \rho_a}{4}\left[ ln\left(\frac{y_{N2}}{y_{N1}}\right)\frac{1}{h_C \alpha_C} + \frac{1}{h_M y_M}\right]$ and $\mathrm{C} = \frac{4Eh^3}{3\pi^3 a^2 (1-\nu^2)}$.

Equation (19) plotted in Fig. 3, which expresses the relationship between the resonant frequency of the system and the rectifying coefficient of the nozzle depicts that the rectification coefficient increases with the decrease of the resonant frequency. The rectification coefficient of the present device based on the resonant frequency measured by experimental work will be presented and calculated in section 4.1.

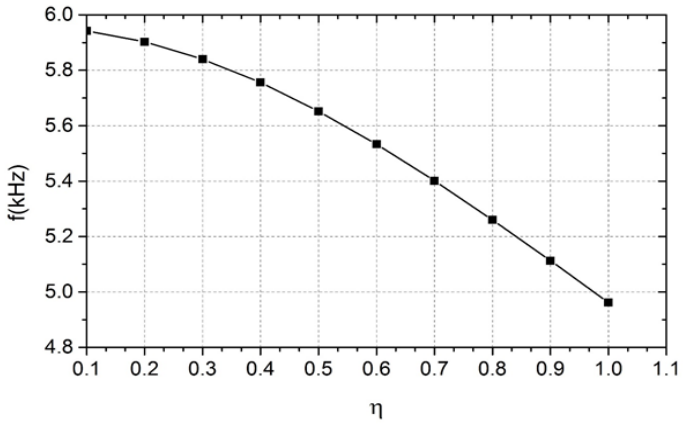


Figure 3. Relationship between the natural frequency (f) and rectification ratio (η) of the nozzle as predicted by Eq. (19)

## 2. 4 ANGULAR RATE SENSING BY HOTWIRE ANEMOMETRY

While the device rotates together with a rotating frame, the Coriolis force deflects the flow in the sensing chamber (see Fig. 4). This deflection is detected by hotwires. Based on the 3D simulation of flow inside a rotating device performed in our last publication [43], an analytical expression is presented in this paper for the sake of discussing in the next sections.

The deflection of flow in the sensing chamber originated from nozzle can be calculated as

$$\overrightarrow{d_\omega} = \iint \vec{a} dt = \iint 2\overrightarrow{V_{flow}} \times \vec{\omega} dt \quad (20)$$

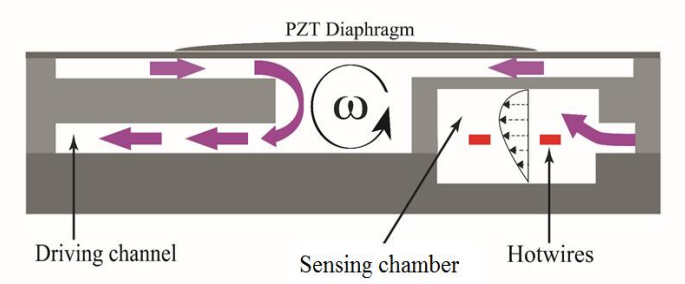


Figure 4 Deflection of air flow under rotating frame is measured by hotwire inside sensing chamber

where $t$ is the time period the air flow shifts from the nozzle to a hotwire; $V_{flow}$ the average velocity calculated by $V_{flow} = x/t$ with $x$ the distance from the nozzle to the hotwire. As a result, the deflection of the air flow inside the chamber on the direction perpendicular to the rotational axis is determined by $d_\omega = \omega x^2/V_{flow}$ .

Let $\beta$ be the profile of velocity gradient of air flow on the cross-section of the sensing chamber at a hotwire, the deflection of air flow can be converted into a variation of air flow velocity as

$$\Delta V_\omega = \beta \cdot d_\omega = \beta\omega \frac{x^2}{V_{flow}}, \tag{21}$$

where the parameters are defined in the nomenclature. When a hotwire heated by an electric current $I$ is subjected to a variation of cooling air velocity ($\Delta V_\omega$), the temperature variation of the hotwire ($\Delta T_{HW\omega}$) is converted into a relative variation of resistance by

$$\Delta R_\omega = \alpha \Delta T_{HW\omega} \tag{22}$$

Substituting Eq. (21) into (22) yields the relationship between the hotwire resistance and the applied angular velocity as follows [38].

$$\Delta R_\omega = \frac{\lambda\pi l\alpha I^2 R_{HW}^2}{(\lambda\pi l Nu - I^2 R_{HW}\alpha)^2} \cdot \frac{nNu}{V_{\text{flow}}^2} \cdot \beta x^2 \omega \tag{23}$$

where $l$ = 3.5 mm , $\alpha = 4500$ ppm/°C, and $R_{HW}$= 7.9 Ω are the typical length, temperature coefficient of the resistance and the reference resistance of the hotwire, respectively; $\lambda = 24.2 \times 10^{-3}$ W/(m K) the thermal conductivity of air; and *Nu* the Nusselt number representing the heat transfer coefficient between air flow and the hotwires [49].

Eqs. (21)-(23) describing the relationship between the applied angular velocity ($\omega$) and the hotwire resistance is linear if the jet flow is created inside the working chamber [38]. The equations will be investigated by experiments where several other design parameters of the system affecting the flow deflection are also found in the next sections.

## 3. EXPERIMENTAL SETUP

A transparent prototype of poly-methyl methacrylate (PMMA) is designed and manufactured as illustrated in Fig. 5. A circular PZT diaphragm with diameter of 20 mm (7BB-20-6, Murata Ltd.) is installed to seal the system using epoxy glue and to form a pump chamber with a depth of 0.3 mm [50]. The dimensions of the present device are 21 × 21 × 2.5 mm (width × length × thickness). Two tungsten hotwires (W-461057, Nillaco Ltd) with length of 3.5 mm and diameter 10 µm each, are placed inside each sensing chamber at distances of 1.0 mm and 2.5 mm downstream from the nozzle. Lead pins (Preci-Dip) are installed in the device and work as hotwire holders. The two hotwires are located at the center of the chamber depth.

The temperature coefficient of resistance measured in temperature controlled chamber (Espec SH-222) is $\alpha \approx 4500$ ppm/°C. The PZT diaphragm vibrates under sinusoidal signals which are created by a function generator (IWATSU SG-4105). A constant current is supplied to hotwires whose voltages are monitored by a TEXIO DC power supplier (PW18-1.8AQ). The ambient environment is maintained at standard room conditions (22–25 °C, 60% RH).

The kinetics of the gyroscope is analyzed using a self-developed turntable which comprises an aluminium disc with diameter of 10cm. The turntable is driven by a direct current motor whose angular velocity is monitored by an integrated encoder (Tsukasa Electric Ltd). The device is connected to the outer circuit through a slip-ring mechanism installed along the center of the turntable, which allows the electrical system working safely while the turntable rotates. The angular rate of turntable, recorded by a PIC18F4520 microcontroller via an encoder, can reach an angular rate of 1900 rpm. During the time-resolved analysis, experimental results are continuously recorded and monitored by a computer system using NI Signal Express-data logging software (National Instrument Ltd.) via NI9234 data acquisition module with a sampling rate

of 25.6 kHz. The turntable is initially calibrated with a standard angular rate sensor ADXRS649 (connected via evaluation board EVAL-ADXRS649Z, Analog Device Ltd.)

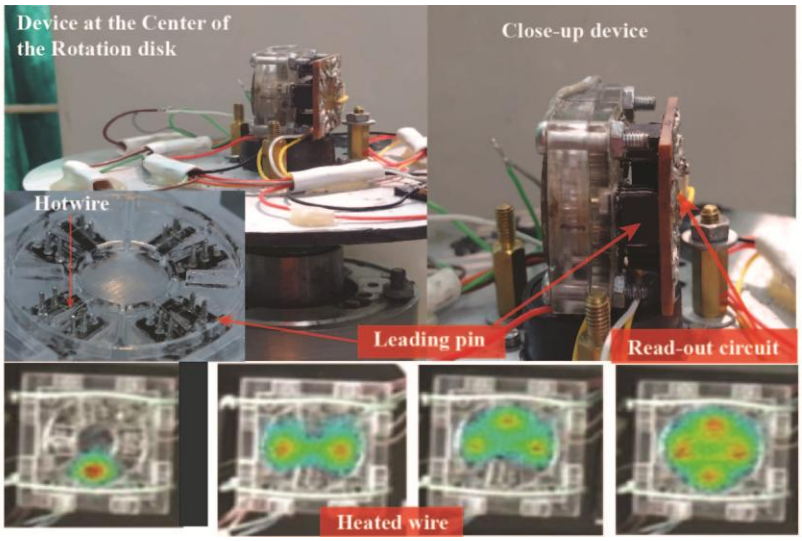


Figure 5. Setup of experiment. Investigation of the inertial effect on flow inside the device installed at the center of turntable with unassembled device (Top Figures) using heated hotwires placed at four different positions (Bottom Figures)

The mechanism of inertial sensing described above is investigated by locating the device at the center of the turntable. In fact, while the turntable rotates, the air flows in the channels parallel to the table's plane are deflected. This reduces the velocity of flows through the hotwires, yields a variance of the temperature and thus the resistance of hotwires as shown in equation (23). Meanwhile, the flows in the channels normal to the table's plane spin around the axis of the turntable. So, if the velocity profiles of flows in these channels are symmetric about the jet flow's axis, the velocities through hotwires do not change.

To prepare the experiment, the heated hotwires are initially observed using a thermal camera (InfReC H2640, Avio Ltd) and the insets of Fig. 5 illustrates the thermal images of hotwires in each working chamber heated with a current $I$ of 0.03 A.

## 4. ANALYSIS OF THE DEVICE PROPERTIES

With the experimental setup described in section 3, the present device is investigated with several criteria including the pumping performance, the natural frequency, the hotwire anemometry and the time-dependent characteristics of the jet flow.

### 4.1 PUMPING PERFORMANCE AND RECTIFICATION RATIO

Figure 6 shows the simulated average velocity of air flow recorded at every time step of 1/20$^{th}$ of the PZT's vibrating period in the sensing chamber at four positions, $x$ = 1.0, 1.5, 2.0, and 2.5 mm from the nozzle. As described in section 2.1, a weak flow which is initially generated in the pump channel propagates to the working chamber. The flow then circulates back to the rectifying nozzle accompanied an increase of its momentum, which amplifies the rectification of the nozzle. This is evidenced by a boost of the flow speed as shown in Fig. 6. After certain circles of rectification, the flow velocity attains a steady state of fluctuation with the oscillation frequency of diaphragm when the air flow expands at a peak velocity (around 3–5 m/s). The simulated velocity of flow is used to investigate the reliability of the experiment in section 4.

With a given voltage of 9 V applied on the PZT diaphragm, experimental results by Fig. 7a show an increase of the output voltage on the hotwires with the increase of the actuating frequency of the PZT. The output voltage then decreases rapidly after reaching a peak value at the frequency of 5.1 kHz. Furthermore, Fig 7a also depicts that while the output voltage through hotwires increases with the increase of current, the characteristics of the output voltage and the actuating frequency of the PZT are independent of the hotwire current. In addition, the relationship between the output voltage of hotwires $V_{HW}$ and driving voltage of the PZT ($V_{PZT}$) is also considered while the system is actuated with the resonant frequency and heated by a current of 0.06 A. Experimental results by Fig. 7b show that the output voltage of hotwires increases with the increase of the driving voltage of the PZT. In other words, the larger deformation of the diaphragm the $V_{PZT}$ creates, the higher speed of air flow will be.

It is worth nothing that results by Fig. 7 are the base to determine (i) the resonant frequency of the present system (5.1 kHz) and (ii) the way to increase the output voltage on hotwires by enhancing the heat transfer through hotwires. Hence,

these results will be used to evaluate the rectification coefficient and to improve the sensing performance of the present device in sections 2.3 and 4.4.

At the resonant frequency of 5.1 kHz, the rectification coefficient of the nozzle in the present circulating system (a closed one) is about 0.9 as illustrated in Fig. 3. This rectification is much higher than ones in opened systems, which theoretically cover from 0.38–0.42 as mentioned in several publications ([51], [52]). This improvement of rectification coefficient achieved owing to the momentum accumulation after each circulation of jet flow from the driving channel to sensing chambers. Hence, the present system allows to generate jet flows at a relatively low actuating voltage on the PZT membrane. So, it is a significant contribution in developing gyroscopes.

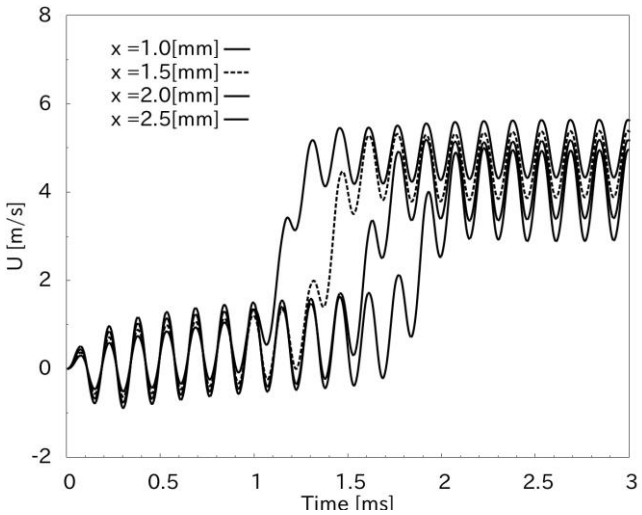


Figure 6 (Simulation) Time-dependent axial velocity of air flow inside a working chamber through several hotwires installed at four positions $x$ = (1.0, 1.5, 2.0, and 2.5 mm) with a deflection of 5 μm of PZT diaphragm. The velocity of air flow is recorded at every time step of 1/20$^{th}$ of the PZT's vibrating period.

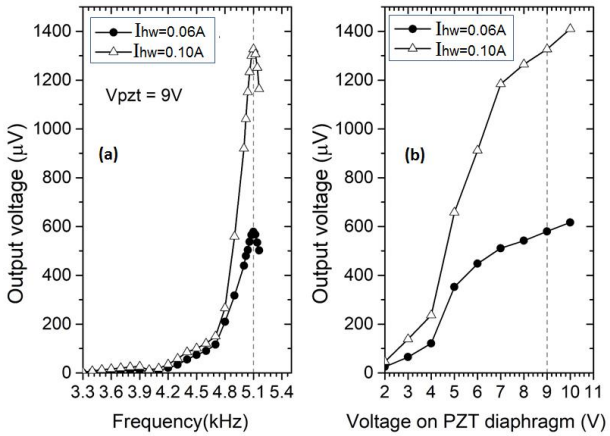


Figure 7 Pumping characteristics obtained by experimenting on the device. (a): the frequency response of the device using an actuating voltage of 9 V on PZT diaphragm for hotwire heated by currents of 0.06 A and 0.1 A; (b): the effect of actuating voltage of PZT diaphragm on the output voltage on hotwire heated by currents of 0.06 A and 0.1 A.

Finally, the transient output voltage plotted at the resonant frequency of the device in Fig.8 depicts that the start-up time for hotwires to reach a stable value of voltage is approximately 5ms. This experimental observation is marginally longer than the simulation result with an order of several milliseconds. This marginal difference results in the effect of imperfections of the device geometry and the delay occurring in the electronic circuits of the system. Furthermore, Fig. 8 also reveals a reasonable correlation between start-up times of output voltage on two hotwires located 1 mm and 2.5 mm from the nozzle in the working chamber. The time delay $\Delta t$ between two hotwires is used to expeditiously estimate the average velocity of flow between them.

Assume that the two hotwires are identical, the average velocity of flow between two hotwires is calculated as the ratio of the distance between the two hotwires (1.5 mm) to the time delay $\Delta t$ (0.49ms). The flow velocity measured by the experiment is 3.06 m/s, which is in good agreement with the numerical results presented in Fig. 6.

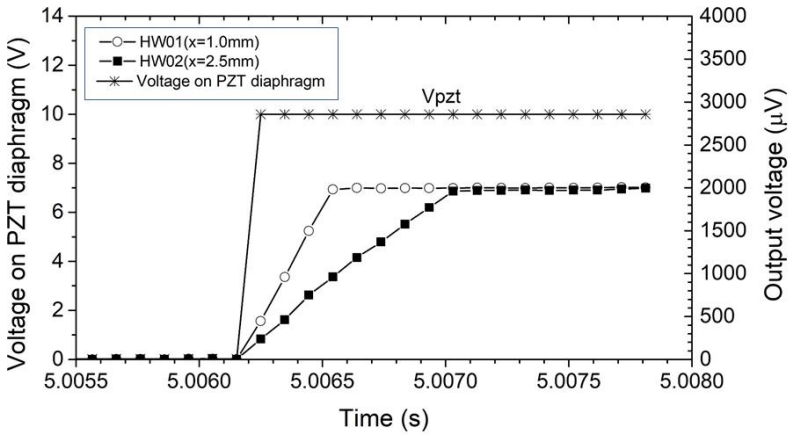


Figure 8 Start-up voltage actuating on PZT diaphragm and output voltage measured on hotwires located at two positions of 1 mm and 2.5 mm from the nozzle by experimental works using an actuating voltage of 10 V on PZT diaphragm.

In the next sections, the sensing performance is evaluated with two different cases where the device is installed at the center and the edge of the turntable.

## 4.2 ANGULAR RATE SENSING PERFORMANCE

In order to analyze the angular rate sensing performance, the device is set-up at the center of a turntable as shown in Fig. 5.

The effect of the symmetry of the device on the sensing performance is studied via the voltage variation on hotwires in the two opposite horizontal chambers (channels 1 and 2) with respect to the turntable angular rate. Results by Fig. 9 depict show that the time evolutions of output voltage on two identical hotwires in two opposing horizontal chambers with respect to angular rate are the same. This indicates that the velocities of air flow in the channels are identical. These results are in good agreement with those observed by a high-speed camera as presented in our recent publication [53].

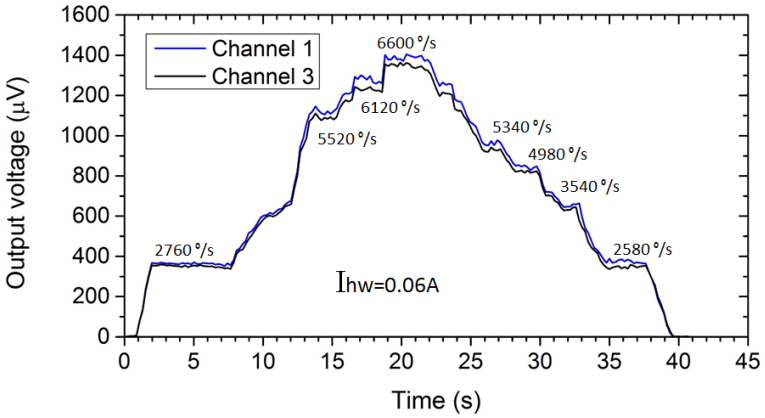


Figure 9. Time-dependent output voltage on hotwires installed at an identical distance from the nozzle in two horizontal channels (channels 1 and 3) for a range of rotation speeds. Device is installed at the center of the turntable and hotwires are heated by a current of 0.06 A.

Meanwhile Fig. 10a presents the variation of output voltage on hotwires installed 2.5 mm from the nozzle in '*the horizontal and vertical chambers*' with respect to the angular speed of the turntable. Results depict that the output voltage linearly increases with the increase of angular speed with a scale factor of 0.26 μVs/° until the speed reaches 900 rpm (5400 °/s). A nonlinear increase of the output voltage observed at higher speeds may correlate with the flow deflection restricted by the wall of chamber as stated in [43]. For example, at the angular speed of 1500 rpm, the measured velocity of flow is $V_{flow}$=3.06 m/s (see section 4.1) and the flow deflection is estimated as $d_\omega = \omega L^2/V_{flow} = 0.33$ mm (nearly a half of the distance from the jet axis to the wall chamber). It can be seen that the output voltage reaches a stable value as the flow deflects toward the wall of the sensing chamber. Moreover, this deflection disappears when the deflection reached a yield value defined as the distance between the jet axis (0, 0, 0) and the wall of chamber (it is 0.75 mm in this work),

The experimental results by Fig. 10a also present a significant difference between the readings in vertical and horizontal channels. This difference can be explained as follows. Since flows in a vertical channels perpendicular to turntable plane are parallel to the rotational axis, they only spin about their longitudinal axis and then do not cause any significant difference of the flow velocity at hotwire positions, i.e. $\overrightarrow{V_{flow}} \times \vec{\omega} \approx 0$. As a result, the output voltage on hotwires in vertical channels is very low with a scale factor of 0.003 μVs/°. Meanwhile, the increasing of output voltage on hotwires in horizontal channels is about 85 times higher than that in vertical channels. In addition, the cross-sensitivity between the two channels is accordingly determined to be 1.2 %.

Figure 10b presents the experimental relationship of the output voltage on hotwires and the actuating voltage applied on the PZT diaphragm while the turntable rotates with a constant angular speed of 1100 rpm (6600 °/s). Results show that the output voltage on hotwires in both vertical and horizontal channels is negligible at low actuating voltages (< 4 V) applied on the PZT diaphragm. The output voltage then rapidly increases when the PZT diagram vibrates with higher voltages. After generated by an actuating voltage of the PZT diagram, the velocity of flow increases quickly with the oscillation of PZT diaphragm. This yields a higher variation of air velocity through hotwires and then an increase of output voltage on hotwires [43].

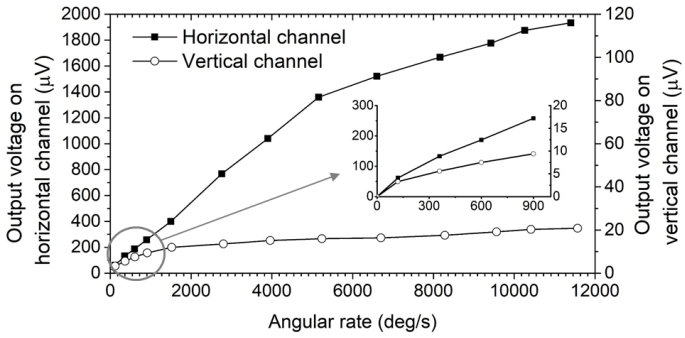


Figure 10a. Output voltage on hotwire versus the angular rate of turntable. Hotwires are installed at equal-distances ($x$ = 2.5 mm) from nozzle in horizontal and vertical channels. Device is located at the center of turntable, using $V_{PZT}$ of 8 V and a heating current of 0.08 A

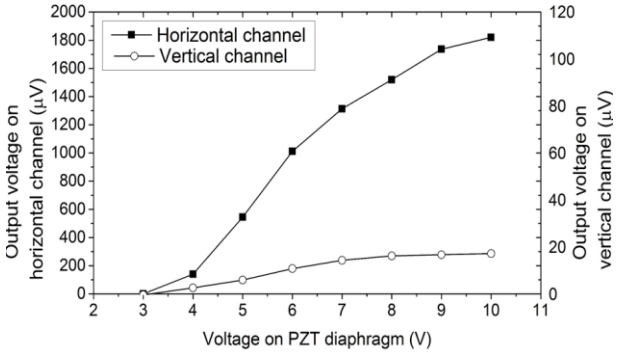


Figure 10b. Output voltage on hotwire versus the actuating voltage applied on PZT diaphragm. Hotwires are installed at equal-distances ($x$ = 2.5 mm) from nozzle in horizontal and vertical channels. Device is located at the center of turntable with an angular velocity of 1100 rpm and a heating current of 0.08 A

### 4.3 Effect of linear acceleration

In order to investigate the effect of linear acceleration on the sensitivity of the system, device is placed at the edge of the turntable whose centripetal acceleration is determined by $a_{linear} = (2\pi n)^2 r_t$, where $n$ and $r_t$ = 4.5 cm are the angular velocity and the radius of the turntable, respectively.

According to [54], the effect of gravity on a jet flow is small because the free jet flow is "floated" in a media. This is confirmed in this work by comparing the output voltages measured on an identical hotwire in the sensing chamber which is set up on the horizontal and vertical directions while the turntable is at rest. In fact, since the difference between these output voltages is very small, the effect of gravity is insignificant in our present device. This experimental observation fits well with our recent publication [26] in which the effect of gravity was only 0.75 °/s/g.

In addition, the effect of linear acceleration is further investigated by installing the present device at the edge of a turntable where a centrifugal acceleration is generated up to 60 times of the gravity acceleration by the turntable's angular speed of 6600 °/s. For this experiment, the time evolution of output voltages measured on hotwires in horizontal and vertical channels for a range of angular speeds of the turntable (2760 °/s - 6600 °/s ) using an actuating voltage $V_{PZT}$ of 8 V is presented in Figs. 11a&b. In comparison with output voltages measured on hotwires in Fig. 10 while the device is set up at the turntable center, the effect of linear acceleration on the sensitivity of the present system is around 0.196 $\mu Vm^{-1}s^2$ for hotwires in the vertical channels. Thus, the effect of gravity acceleration can be linearly approximated as 1.96 $\mu Vg^{-1}$, which is equivalent to 0.26% of the full-scale measurement as given in Fig. 10a.

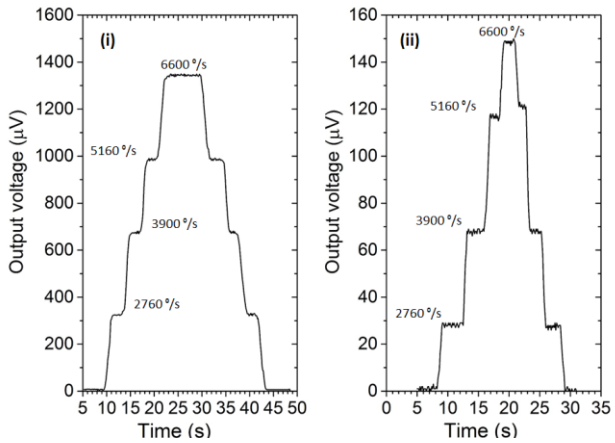


Figure 11a Real time output voltage recorded on hotwires which are installed in horizontal channel (i) and vertical channel (ii) with actuating voltage $V_{PZT}$ = 8 V and using a heating current of 0.08 A. Device is located at the edge of turntable to impose a linear acceleration

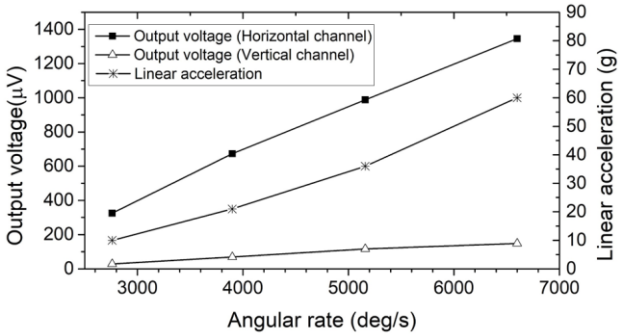


Figure 11b Relationships of the output voltage on hotwires and the linear acceleration with respect to the angular velocity of the turntable (using data in Fig. 11a)

### 4.4 Effect of heating current

The effect of the heating current on the sensitivity of the device is studied for several heating currents ($I$ = 0.046, 0.06, and 0.08 A) with an actuating voltage of 10 V for the diaphragm. Results presented in Fig. 12 show that the stronger current hotwires are heated by, the more sensitive the device is. By the use of Eq. (23), the output voltage on hotwires can be determined with respect to the angular speed of turntable and heating current. For example, with an angular velocity of 1570 rpm (9420 °/s), the output voltage on hotwires heated by a current of 0.08 A is 2.63 times higher than that with a heating current of 0.06 A. Thus, the heating current can be used to expedite the experiment.

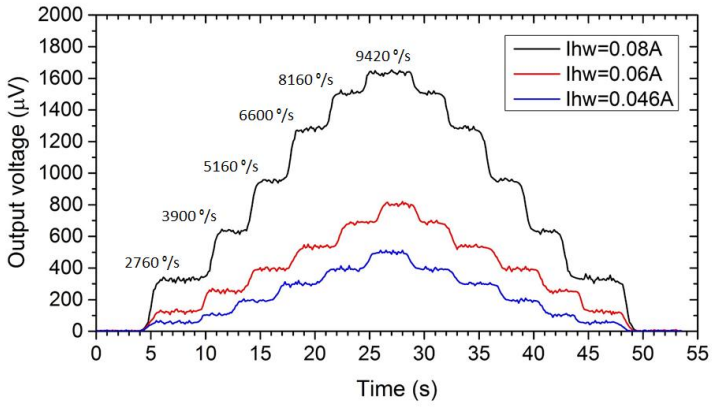


Figure 12 Real time output voltage recorded on a hotwire installed at distance of 2.5 mm from nozzle in the horizontal channel parallel to the turntable plane for several angular velocities speeds (0, 460, 860, 1100, 1360, and 1570 rpm) using several heating currents (0.046, 0.06 and 0.08 A) and an actuating voltage of 10 V on PZT diaphragm. Device is placed at the edge of the turntable.

### 4.5 Effect of hotwire position

The output voltage on hotwires of a rotating device depends on the hotwire positions. The experimental results in Fig. 13 show that the output voltage measure at hotwires located farther from the nozzle is more sensitive and this observation can be demonstrated by Eqs. (21) and (23). For example, the scale factor of output voltage of hotwire installed 1.0 mm from the nozzle in the horizontal channel is 0.106 μVs/°, which is about 53 % of that on the hotwire located 2.5 mm from the nozzle (with a scale factor of 0.201 μVs/°). Furthermore, under the influence of linear acceleration as mentioned in section 4.3, the scale factor of output voltage on hotwires in the vertical channel is also dependant on the position of hotwires.

Experimental results also depict that the output voltage on a hotwire increases with the increase of angular speed of the turntable until reaches a stable state corresponding to a particular position of the hotwire in channels. As illustrated in Fig. 13, when the turntable rotates with angular rate of 1700 rpm (10200 °/s ), the output voltages on hotwires located 2.5 mm and 1 mm from the nozzle in the horizontal channel reach the stable values of 1800 μV and 1300 μV, respectively. Meanwhile, the output voltages of 190 μV and 100 μV are found measured on hotwires at 2.5 mm and 1.0 mm from the nozzle in the vertical channel, respectively with angular velocity of 1350 rpm (8100 °/s ). The results imply that the air flow is not further deflected by the turntable's rotation because of the geometrical restriction of the sensing chamber.

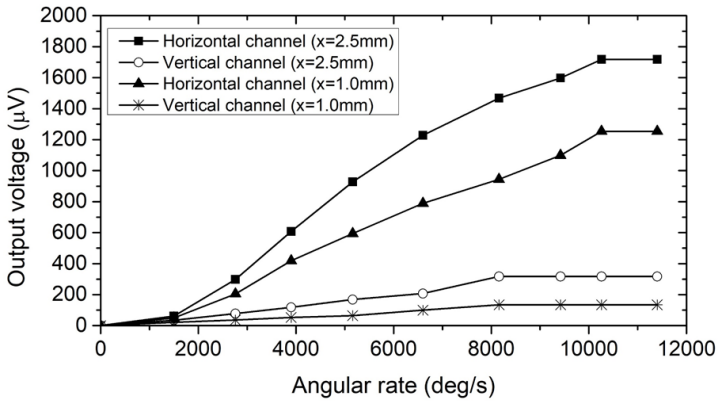


Figure 13 Effect of the rotational speed of turntable on the output voltage on hotwires installed at two locations, 1 mm and 2.5 mm away from the nozzle, in vertical and horizontal channels. Device is placed at the edge of turntable

Overall, the sensing performance of the present device is in the same order as those by recent publications. For example, the scale factors of thermal expansion and vortex based sensors were reported 0.61 μVs/° [34] and 0.16 μVs/° [37] while the scale factor of the present device is about 0.26 μVs/° (section 4.2). Thus, all sensors are in the same group of rate grade as classified in [55]. However, as discussed in the last sections, the sensing performance of the present device is not much affected by the linear acceleration (or gravity acceleration), especially for fluidic gyroscopes. Furthermore, it is worth noting that the measurement in our experimental work examines the behavior of a jet flow on a hotwire in each chamber, not a pair of them as normally being performed in conventional sensing circuit. Should the linear acceleration (or gravity) affects the flows similarly in all of four chambers, by simply connecting two hotwires in two each opposite sensing chambers to form a half Wheatstone bridge circuit, the sensitivity of angular rate sensing is easily enhanced and the effect of linear acceleration is effectively cancelled out [38].

The performance of the present device of this work can be further improved by introducing our several techniques developed recently, for example, the use of silicon doped hotwire in place of tungsten [38], [40], and further boosted with a p-n junction temperature sensing element [56]. Furthermore, the minimum angular speed achieved in this work is not limited by the device mechanism but the stability of turntable. By balancing the system and improving the rigidity of the frame, we are successful to reduce the turntable revolution to 20 rpm (120 °/s ). However, the present configuration is not enough stable to rotate very slowly (less than 360 °/s ) if the device is installed at the edge of the turntable. It is worth noting that the evaluation of the sensor performance for angular rate lower than 360 °/s is necessary because it yields a relevant tune of several design parameters. Hence, an improved turntable is under development and will be presented in our next publication.

Finally, so far, we cannot be able to completely eliminate the effect of linear acceleration of 0.196 $\mu Vm^{-1}s^2$ on the sensor performance. In reality, it is necessary to integrated in the present system a multi-axis accelerometer which acts as a reference device to overcome this issue. The work is on process in our laboratory and would be reported in our next paper.

## 5. CONCLUSION

In this paper, we report a closed device of millimeter-scale that can generate multiple jet flows in the form of two perpendicular pairs using a PZT diaphragm. The characteristics of flows are numerically simulated and then verified by experimental works. Simulating and experimental results by the work show that the identical flows are generated in the four sensing chambers. The performance of the device can be customized by either fluidic parameters such as the driving voltage on the diaphragm and/or heat transfer parameters such as the heating current. As jet flows are quantitatively measured on hotwires integrated in the device, the system is robust and ready-to-use. The cross-sensitivity, effects of linear acceleration, actuating voltage on the diaphragm, heating power and position of hotwires on the device's performance are also investigated. Results by testing the device on a rotating frame show the potential of the present device as a fluidic gyroscope. Moreover, by arranging hotwires in a symmetric pair with opposite output voltages, the performance of the device can be improved using conventional electronic circuits. Finally, since the device is assembled by laminated parts, it is compatible with a conventional microfabrication process, yielding a significant cost reduction.


## ACKNOWLEDGEMENT

This research is funded by Vietnam National Foundation for Science and Technology Development (NAFOSTED) under grant number 107.01-2015.22


## Reference


[1] M. Krishnan, N. Agrawal, M. A. Burns, and V. M. Ugaz, "Reactions and fluidics in miniaturized natural convection systems.," *Anal. Chem.*, vol. 76, no. 21, pp. 6254–65, Nov. 2004.

[2] S.-I. Ohira and K. Toda, "Miniature liquid flow sensor and feedback control of electroosmotic and pneumatic flows for a micro gas analysis system.," *Anal. Sci.*, vol. 22, no. 1, pp. 61–65, 2006.

[3] X. Li *et al.*, "Improving mixing in microbioreactors," *Chem. Eng. Sci.*, vol. 63, no. 11, pp. 3036–3046, Jun. 2008.

[4] A. P. Sudarsan and V. M. Ugaz, "Fluid mixing in planar spiral microchannels.," *Lab Chip*, vol. 6, no. 1, pp. 74–82, Jan. 2006.

[5] T. X. Dinh, D. B. Lam, C.-D. Tran, T. T. Bui, P. H. Pham, and V. T. Dau, "Jet flow in a circulatory miniaturized system using ion wind," *Mechatronics*, vol. 47, no. September, pp. 126–133, Nov. 2017.

[6] D. Jang and K. Lee, "Flow characteristics of dual piezoelectric cooling jets for cooling applications in ultra-slim electronics," *Int. J. Heat Mass Transf.*, vol. 79, pp. 201–211, Dec. 2014.

[7] H. K. K. Ma, H. C. C. Su, and W. F. F. Luo, "Investigation of a piezoelectric fan cooling system with multiple magnetic fans," *Sensors Actuators, A Phys.*, vol. 189, pp. 356–363, Jan. 2013.

[8] L. Meyer *et al.*, "A silicon-carbide micro-capillary pumped loop for cooling high power devices," in *Ninteenth Annual IEEE Semiconductor Thermal Measurement and Management Symposium, 2003.*, 2003, pp. 364–368.

[9] V. T. Dau, T. X. Dinh, and T. T. Bui, "Jet flow generation in a circulatory miniaturized system," *Sensors Actuators B Chem.*, vol. 223, pp. 820–826, 2015.

[10] K. D. Dorfman, M. Chabert, J.-H. Codarbox, G. Rousseau, P. de Cremoux, and J.-L. Viovy, "Contamination-free continuous flow microfluidic polymerase chain reaction for quantitative and clinical applications.," *Anal. Chem.*, vol. 77, no. 11, pp. 3700–4, Jun. 2005.

[11] A. Baïri, J. M. García de María, N. Laraqi, and N. Alilat, "Free convection generated in an enclosure by alternate heated bands. Experimental and numerical study adapted to electronics thermal control," *Int. J. Heat Fluid Flow*, vol. 29, no. 5, pp. 1337–

1346, 2008.
[12] L. Y. Yeo, H. C. Chang, P. P. Y. Chan, and J. R. Friend, “Microfluidic devices for bioapplications,” *Small*, vol. 7, no. 1, pp. 12–48, 2011.
[13] V. Studer, A. Pepin, Y. Chen, and A. Ajdari, “An integrated AC electrokinetic pump in a microfluidic loop for fast and tunable flow control.,” *Analyst*, vol. 129, no. 10, pp. 944–949, 2004.
[14] Y. H. Seo, H. J. Kim, W. K. Jang, and B. H. Kim, “Development of active breathing micro PEM fuel cell,” *Int. J. Precis. Eng. Manuf. Technol.*, vol. 1, no. 2, pp. 101–106, 2014.
[15] X. Yang, Z. Zhou, H. Cho, and X. Luo, “Study on a PZT-actuated diaphragm pump for air supply for micro fuel cells,” *Sensors Actuators, A Phys.*, vol. 130–131, no. SPEC. ISS., pp. 531–536, Aug. 2006.
[16] S. Liu and R. Zhu, “Micromachined Fluid Inertial Sensors,” *Sensors*, vol. 17, no. 2, p. 367, 2017.
[17] N.-C. Tsai, J.-S. Liou, C.-C. Lin, and T. Li, “Suppression of dynamic offset of electromagnetic drive module for micro-gyroscope,” *Mech. Syst. Signal Process.*, vol. 25, no. 2, pp. 680–693, Feb. 2011.
[18] H. Cao, H. Li, J. Liu, Y. Shi, J. Tang, and C. Shen, “An improved interface and noise analysis of a turning fork microgyroscope structure,” *Mech. Syst. Signal Process.*, vol. 70–71, pp. 1209–1220, Mar. 2016.
[19] H. Cao *et al.*, “Sensing mode coupling analysis for dual-mass MEMS gyroscope and bandwidth expansion within wide-temperature range,” *Mech. Syst. Signal Process.*, vol. 98, pp. 448–464, Jan. 2018.
[20] V. T. Dau, T. X. Dinh, and S. Sugiyama, “A MEMS-based silicon micropump with intersecting channels and integrated hotwires,” *J. Micromechanics Microengineering*, vol. 19, no. 12, p. 125016, Dec. 2009.
[21] Z. Zhang, J. Kan, S. Wang, H. Wang, J. Wen, and Z. Ma, “Flow rate self-sensing of a pump with double piezoelectric actuators,” *Mech. Syst. Signal Process.*, vol. 41, no. 1–2, pp. 639–648, Dec. 2013.
[22] V. T. Dau and T. X. Dinh, “Numerical study and experimental validation of a valveless piezoelectric air blower for fluidic applications,” *Sensors Actuators B Chem.*, vol. 221, pp. 1077–1083, Jul. 2015.
[23] K. Mori, H. Yamamoto, K. Takemura, S. Yokota, and K. Edamura, “Dominant factors inducing electro-conjugate fluid flow,” *Sensors Actuators A Phys.*, vol. 167, no. 1, pp. 84–90, 2011.
[24] K. Takemura, S. Yokota, M. Suzuki, K. Edamura, H. Kumagai, and T. Imamura, “A liquid rate gyroscope using electro-conjugate fluid,” *Sensors Actuators A Phys.*, vol. 149, no. 2, pp. 173–179, 2009.
[25] Y. Ogawa, S. Yokota, K. Edamura, and K. Takemura, “A Dual-Axis Liquid Micro Rate Gyroscope Using an Electro-Conjugate Fluid,” *Trans. JAPAN Soc. Mech. Eng. Ser. C*, vol. 77, no. 773, pp. 204–211, 2011.
[26] D. V. Dao, V. T. Dau, T. Shiozawa, and S. Sugiyama, “Development of a Dual-Axis Convective Gyroscope With Low Thermal-Induced Stress Sensing Element,” *J. Microelectromechanical Syst.*, vol. 16, no. 4, pp. 950–958, Aug. 2007.
[27] Ricardo Dao, Denny E. Morgan, Harold H. Kries, and David M. Bachelder, “Convective accelerometer and inclinometer,” US5581034 A, 1996.
[28] Q. Li *et al.*, “Sustained growth of ultralong carbon nanotube arrays for fiber spinning,” *Adv. Mater.*, vol. 18, no. 23, pp. 3160–3163, 2006.
[29] R. Zhu, H. Ding, Y. Su, and Y. Yang, “Modeling and experimental study on characterization of micromachined thermal gas inertial sensors,” *Sensors*, vol. 10, no. 9, pp. 8304–8315, 2010.
[30] S. Liu and R. Zhu, “Dead-beat control based thermal compensation for micromachined thermal gas gyroscope,” *Sensors Actuators A Phys.*, Sep. 2017.
[31] V. T. Dau, D. Viet Dao, and S. Sugiyama, “A 2-DOF convective micro accelerometer with a low thermal stress sensing element,” *Smart Mater. Struct.*, vol. 16, no. 6, pp. 2308–2314, Dec. 2007.
[32] R. Zhu, S. Cai, H. Ding, Y. J. Yang, and Y. Su, “A micromachined gas inertial sensor based on thermal expansion,” *Sensors Actuators, A Phys.*, vol. 212, pp. 173–180, 2014.
[33] R. Zhu, H. Ding, Y. Su, and Y. Yang, “Modeling and experimental study on characterization of micromachined thermal gas inertial sensors.,” *Sensors (Basel).*, vol. 10, no. 9, pp. 8304–15, 2010.
[34] J. Bahari, R. Feng, and A. M. Leung, “Robust MEMS Gyroscope Based on Thermal Principles,” *J. Microelectromechanical Syst.*, vol. 23, no. 1, pp. 100–116, Feb. 2014.
[35] R. Feng, J. Bahari, J. D. Jones, and A. M. Leung, “MEMS thermal gyroscope with self-compensation of the linear acceleration effect,” *Sensors Actuators, A Phys.*, vol. 203, pp. 413–420, 2013.
[36] H. Chang, P. Zhou, X. Gong, J. Xie, and W. Yuan, “Development of a tri-axis vortex convective gyroscope with suspended silicon thermistors,” in *2013 IEEE SENSORS*, 2013, pp. 1–4.
[37] H. Chang, P. Zhou, Z. Xie, X. Gong, Y. Yang, and W. Yuan, “Theoretical modeling for a six-DOF vortex inertial sensor and experimental verification,” *J. Microelectromechanical Syst.*, vol. 22, no. 5, pp. 1100–1108, Oct. 2013.
[38] V. T. Dau, D. V. Dao, T. Shiozawa, H. Kumagai, and S. Sugiyama, “Development of a dual-axis thermal convective gas gyroscope,” *J. Micromechanics Microengineering*, vol. 16, no. 7, pp. 1301–1306, Jul. 2006.
[39] V. T. Dau, T. X. Dinh, D. V. Dao, and S. Sugiyama, “Design and Simulation of a Novel 3-DOF MEMS Convective Gyroscope,” *IEEJ Trans. Sensors Micromachines*, vol. 128, no. 5, pp. 219–224, May 2008.
[40] V. T. Dau, D. V. Dao, T. Shiozawa, H. Kumagai, and S. Sugiyama, “A Single-Axis Thermal Convective Gas Gyroscope,” *Sensors Mater.*, vol. 17, no. 8, pp. 453–463, 2005.
[41] T. X. Dinh and Y. Ogami, “A Principle to Generate Flow for Thermal Convective Base Sensors,” *J. Fluids Eng.*, vol. 131, no. 4, p. 41401, Apr. 2009.
[42] V. T. Dau, T. Otake, T. X. Dinh, and S. Sugiyama, “Design and fabrication of convective inertial sensor consisting of 3DOF gyroscope and 2DOF accelerometer,” in *TRANSDUCERS 2009 - 2009 International Solid-State Sensors, Actuators and Microsystems Conference*, 2009, pp. 1170–1173.
[43] P. T. Hoa, T. X. Dinh, and V. T. Dau, “Design Study of Multidirectional Jet Flow for a Triple-Axis Fluidic Gyroscope,” *IEEE Sens. J.*, vol. 15, no. 7, pp. 4103–4113, Jul. 2015.
[44] Y. Ai, X. Luo, and S. Liu, “Design and modeling of micromachined thermal convective gyroscope with bidirectional jets,” in *Proceedings of the Electronic Packaging Technology Conference, EPTC*, 2007, vol. 0, no. 2, pp. 3–7.
[45] G. Kock, P. Combette, B. Chariot, A. Giani, M. Schneider, and C. Gauthier-Blum, “Study and realization of a fluidic thermal gyrometer,” in *2017 Symposium on Design, Test, Integration and Packaging of MEMS/MOEMS (DTIP)*, 2017, pp. 1–5.

[46] H. T. Phan, T. X. Dinh, and V. T. Dau, “Development of a jet-generator and its application to angular rate sensor,” in *2015 China Semiconductor Technology International Conference*, 2015, pp. 1–3.
[47] S. Timoshenko and S. Woinowsky-Krieger, *Theory of Plate and Shells*, 2nd ed. New York, NY, USA: McGraw-Hill, 1959.
[48] T. X. Dinh, N. T. M. Le, V. T. Dau, and Y. Ogami, “A dynamic model for studying valveless electromagnetic micropumps,” *J. Micromechanics Microengineering*, vol. 21, no. 2, p. 25015, Feb. 2011.
[49] D. C. Collis and M. J. Williams, “Two-dimensional convection from heated wires at low Reynolds numbers,” *J. Fluid Mech.*, vol. 6, no. 3, p. 357, Oct. 1959.
[50] L. Murata Manufacturing, “Piezoelectric Diaphragms, Murata Manufacturing Co., Ltd.,” 2016. [Online]. Available: http://www.murata.com/en-sg/products/sound/diaphragm.
[51] E. Stemme and G. Stemme, “A valveless diffuser/nozzle-based fluid pump,” *Sensors Actuators A. Phys.*, vol. 39, no. 2, pp. 159–167, 1993.
[52] K. S. Yang, T. F. Chao, I. Y. Chen, C. C. Wang, and J. C. Shyu, “A comparative study of nozzle/diffuser micropumps with novel valves,” *Molecules*, vol. 17, no. 2, pp. 2178–2187, 2012.
[53] T. T. Bui, T. X. Dinh, P. T. Hoa, and V. T. Dau, “Study on the PZT Diaphragm Actuated Multiple Jet Flow in a Circulatory Miniaturized System,” in *IEEE Sensor conference 2015*, 2015, pp. 3–6.
[54] S. B. Pope, *Turbulent flows*. Cambridge University Press, 2000.
[55] N. Yazdi, F. Ayazi, and K. Najafi, “Micromachined inertial sensors,” *Proc. IEEE*, vol. 86, no. 8, pp. 1640–1659, 1998.
[56] Van ThanhDau, D. V. Dao, T. Shiozawa, and S. Sugiyama, “Convective Gas Gyroscope Based on Thermo-Resistive Effect in Si P-N Junction,” in *TRANSDUCERS 2007 - 2007 International Solid-State Sensors, Actuators and Microsystems Conference*, 2007, pp. 2525–2528.